Journal of Applied Polymer Science

Combination of Double-Modified Clay and Polypropylene-*graft*-Maleic Anhydride for the Simultaneously Improved Thermal and Mechanical Properties of Polypropylene

Yuanyuan Xu,[1,2] Zhenghong Guo,[2] Zhengping Fang,[1,2] Mao Peng,[1] Lie Shen[1]

[1]MOE Key Laboratory of Macromolecular Synthesis and Functionalization, Institute of Polymer Composites, Department of Polymer Science and Engineering, Zhejiang University, Hangzhou 310027, China

[2]Laboratory of Polymer Materials and Engineering, Ningbo Institute of Technology, Zhejiang University, Ningbo 315100, China

Correspondence to: M. Peng (E-mail: pengmao@zju.edu.cn)

ABSTRACT: Double-modified montmorillonite (MMT) was first prepared by covalent modification of MMT with 3-aminopropyltriethoxysilane and then intercalation modification by tributyl tetradecyl phosphonium ions. The obtained double-modified MMT was melt compounded with polypropylene (PP) to obtain nanocomposites. The dispersion of the double-modified MMT in PP was found to be greatly improved by the addition of PP-*graft*-maleic anhydride (PP-*g*-MA) as a "compatibilizer," whose anhydride groups can react with the amino groups on the surface of the double-modified MMT platelets and thus improve the dispersion of MMT in PP. Fourier transform infrared, X-ray diffraction, transmission electron microscopy, thermogravimetric analysis, scanning electron microscopy, and tensile test were used to characterize the structure of the double-modified MMT, morphology, and the thermal and mechanical properties of the nanocomposites. The results show that PP-*g*-MA promotes the formation of exfoliated/intercalated morphology and obviously increases the thermal properties, tensile strength, and Young's modulus of the PP/double-modified MMT nanocomposites. © 2012 Wiley Periodicals, Inc. J. Appl. Polym. Sci. 000: 000–000, 2012

KEYWORDS: polypropylene; silane coupling agent; polypropylene-*graft*-maleic anhydride; clay; nanocomposites; blending

Received 30 January 2012; accepted 9 June 2012; published online
DOI: 10.1002/app.38178

INTRODUCTION

Layered silicates have been a focus of research interests in material science and engineering in the last two decades because of their unique structure and mechanical properties, in which montmorillonite (MMT) is one of the most widely investigated layered silicates for polymeric nanocomposites. Since the first polyamide 6/MMT nanocomposite was prepared by a group at the Toyota Research Center in Japan,[1] various polymer/MMT nanocomposites with poly(ethylene terephthalate),[2] poly(methyl methacrylate),[3] and epoxy resins[4–6] as the matrices have been reported up to date. Because pristine MMT is intrinsically hydrophilic and only miscible with a few hydrophilic polymers, it must be modified to become miscible with hydrophobic polymers. Both ion exchange with cationic surfactants and covalent functionalization of the silicate layers have been used for the modification of MMT. The intercalation of cationic ions into the interlayer of MMT has been widely reported.[7–10] Alkyl phosphonium, alkyl pyridinium, and dialkyl imidazolium surfactants are typical intercalating agents for the preparation of hydrophobic and highly thermally stable organophilic MMT.[11] Wang[12] et al. and Chow and Neoh,[13] however, demonstrated that sodium MMT (Na-MMT) can also be directly modified by a silane coupling agent, which is covalently bonded to the surface of MMT platelets and facilitates the exfoliation of MMT in polymer/MMT nanocomposites.

On the other hand, polypropylene (PP) is one of the most widely used polyolefins. Because of its nonpolar backbone, it is difficult to obtain PP/MMT nanocomposites without further modification. Manias et al.[14] reported two ways to achieve nanocomposite formation: (1) by introducing functional groups in PP and using common alkylammonium MMTs and (2) by using neat/unmodified PP and a semifluorinated surfactant modification for the MMT. When organoammonium-treated MMT is melt blended with PP, better dispersion was achieved using PP-*graft*-maleic anhydride (PP-*g*-MA) as a compatibilizer, which can enhance the intercalation of the polymer chains with the silicate gallery.[15–17] Liaw et al.[18] reported a compound coupling compatibilizer through condensation of the amino groups of 3-aminopropyltriethoxysilane (APTS) with the anhydride groups of MA moieties in PP-*g*-MA, which is capable of

forming chemical bonding with the MMT while maintaining the compatibility with the PP. However, the reaction was conducted in an organic solvent to promote the dispersion of MMT, which prevents the scale-up application of this method.

In this article, we report a novel double-modified MMT by first covalent modification of MMT by a silane coupling agent and then ionic exchange of tributyl tetradecyl phosphonium chloride (TTPC) for preparing PP/MMT nanocomposites by melt compounding. The coupling agent molecules are covalently bonded to the surface of MMT platelets, and TTPC increases the hydrophobicity of MMT and further improves the dispersibility of MMT in PP, both of which are positive to the mechanical properties of the final nanocomposites. Furthermore, the amino groups on the surface of the MMT platelets can react with the anhydride groups of PP-*g*-MA during melt blending. The effect of PP-*g*-MA on the dispersion of the double-modified MMT in PP matrix and the thermal behavior and mechanical properties of PP/MMT nanocomposites were also investigated.

EXPERIMENTAL

Materials

APTS was purchased from Yaohua Chemical Plant, Shanghai, China. TTPC was purchased from Jiachen Chemical, Shanghai, China. PP (T300) with a melt flow rate (MFR) of 3.0 g/10 min (230°C, 2.16 kg) was purchased from Yangzi Petrochemical, Nanjing, China. Pristine Na-MMT, with a cation exchange capacity of 100 mmol/100 g, was supplied by Fenghong, Zhejiang, China. PP-*g*-MA, with a MFR of 150 g/10 min and a MA content of 1 wt %, was provided by Rizhishen New Technology Development, Shanghai, China. Other chemicals were of analytical grade and used without further purification.

Preparation of Double-Modified MMT

To obtain the double-modified MMT, protonated APTS was first intercalated into the intergallery of MMT by cation exchange and then grafted on the surface of the MMT sheets via the condensation reaction of silanol groups. The APTS-modified MMT was deprotonated with NaOH, and then TTPC was introduced into the intergallery of APTS-modified MMT by ion exchange. In detail, pristine MMT was first dried in a vacuum oven at 110°C for 6 h to remove free water. Then, 10 g of dried MMT and 150 mL of alcohol were added into a 250-mL three-necked flask and continuously stirred for 2 h. About 0.67 g of acetic acid and 2.28 g of APTS were dissolved in 50 mL of alcohol and then mixed with the MMT suspension at 70°C and stirred for 16 h. The modified MMT was filtered, and then the precipitate was washed three times by alcohol. The modified MMT was added into a 250-mL three-necked flask with 100 mL of alcohol and 1 mL of deionized water and stirred for 4 h at 70°C. The modified MMT was filtered and washed three times by alcohol and then dried at 80°C for 24 h. The product was named as NH_3-MMT. About 10 g of NH_3-MMT and 0.4 g of NaOH were mixed in 200 mL of deionized water/alcohol (1 : 1 by weight) in a 500-mL three-necked flask for 20 min. The mixture was filtered, washed, and then dried at 80°C for 24 h. The dried product was named as NH_2-MMT. About 10 g of NH_2-MMT and 4.74 g of TTPC were mixed with 200 mL of deionized water/alcohol (1 : 1 by weight) in a 250-mL three-necked flask and stirred for 20 h at 70°C. Then, the product was filtered, and the precipitate was washed three times by deionized water/alcohol (1 : 1 by weight) and deionized water. The precipitate was dried at 80°C for 24 h. The collected product, that is, the double-modified clay, named as P-NH_2-MMT, was then ground into powder. On the other hand, a control sample of P-MMT was prepared by cationic exchange between MMT and TTPC in aqueous solution.

Table I. Sample code and Compositions of the Nanocomposites

Sample code	PP (wt %)	PP-*g*-MA (wt %)	P-NH_2-MMT (wt %)	P-MMT (wt %)
PP	100	/	/	/
PP-0	97	/	3	/
PP-2	95	2	3	/
PP-4	93	4	3	/
PP-6	91	6	3	/
PP-P-6	91	6	/	3

Preparation of PP/MMT Nanocomposites

The nanocomposites were prepared by melt compounding at 180°C in a ThermoHaake Polydrive with a screw speed of 60 rpm, and the mixing time for all samples was 8 min. The mixed samples were transferred into a mold, heated at 180°C for 10 min, and then pressed at 15 MPa for 5 min, followed by cooling to room temperature. The sample code and the compositions are given in Table I.

Characterization

Fourier transform infrared (FTIR) spectroscopy was performed on a VECTOR 22 FTIR Spectrometer (Bruker, Leipzig, Germany) using KBr pellets with a resolution of 4 cm^{-1}. Powder X-ray diffraction (XRD) measurements were conducted on a Rigaku X-ray generator (Cu Kα radiation with $\lambda = 1.54$ Å) at room temperature. The diffraction patterns were recorded at the scattering angles from 0.5° to 10° at a scanning rate of 2° min^{-1}. The samples of MMT for XRD were obtained by filtration, whereas the samples of PP/MMT hybrids were compression molded at 180°C to 25 mm in diameter with a thickness of 1.1 mm. The thermogravimetric analysis (TGA) was carried out on a TG209F1 thermal analyzer (NETZSCH, Germany) with a constant scanning rate of 20°C min^{-1}. Samples were examined in air atmosphere with a heating range from 40 to 600°C and in nitrogen atmosphere with a heating range from 40 to 800°C. The activation energy (E_a) for the degradation of samples in air atmosphere is calculated from TGA by the integral method based on the Horowitz–Metzger equation:[19–21]

$$\ln\left[\ln(1-\alpha)^{-1}\right] = \theta \cdot E_a/RT_{\max}^2, \quad (1)$$

where α is defined as the decomposition ratio, that is, $\alpha = (m_0 - m)/(m_0 - m_\infty)$, where m is actual weight at time t, m_0 is the initial weight, and m_∞ is the weight at the end of degradation. θ is the difference between T and $T_{\max}$, and R is the gas constant. The value of E_a is obtained from the slope of the straight line of $\ln[\ln(1-\alpha)^{-1}]$ versus θ.

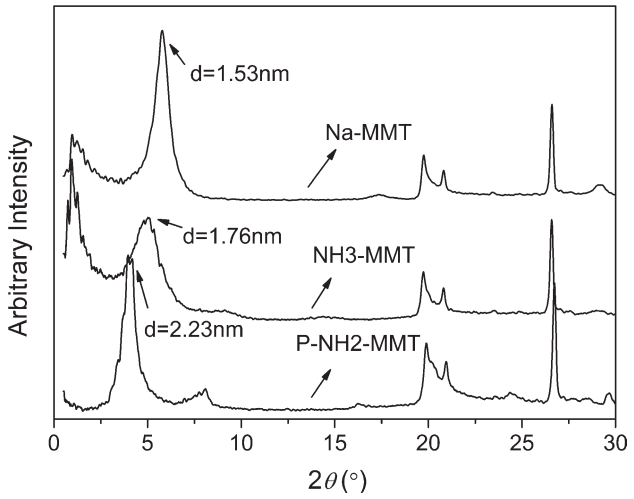

Figure 1. XRD patterns of MMT, NH_3-MMT, and P-NH_2-MMT.

Transmission electron microscopy (TEM) image was obtained using a JEM-1200EX TEM. The ultrathin slides were obtained from thermal-molded samples, using a microtome equipped with a diamond knife. The slides of about 70–90 nm in thickness were collected in a trough filled with water, placed on 200 mesh copper grids, and observed by TEM at an accelerating voltage of 120 kV. Scanning electron microscopy (SEM) observation of the char residues was carried out on an S-4800 microscope under an accelerating voltage of 5 kV. Samples used for the char analysis were 30 mm × 5.0 mm × 3.5 mm in size and were placed in a muffle furnace at 380°C for 5 min. The tensile tests were carried out on a Universal Materials Testing Machine (XWW-20KN, Jinjian, Chengde, China) with a crosshead speed of 50 mmmin^{-1}. The specimens were prepared according to ASTM (D-638). All the tests were performed at 23°C ± 2°C. The results were the average values of at least five measurements.

RESULTS AND DISCUSSION

Effects of Silane Modification

XRD Patterns. Figure 1 shows the XRD patterns of the pristine MMT and the modified MMT. MMT shows a strong peak at 5.77°, corresponding to a basal space (d_{001}) of 1.53 nm. In the case of NH_3-MMT, the peak is at 5.01°, corresponding to a basal space (d_{001}) of 1.76 nm, which is 0.23 nm larger than that of MMT. This should be attributed to the intercalation of silane coupling agent APTS in the intergallery of silicate layers. The peak of P-NH_2-MMT further shifts to a lower 2θ value of 3.96°, corresponding to a basal space (d_{001}) of 2.23 nm. Interestingly, the basal space (d_{001}) of P-NH_2-MMT was 0.47 nm larger than that of NH_2-MMT, indicating that TTP ions enter the interlayer of MMT and expand the basal space. The results also indicate that the MMT platelets were not crosslinked by APTS during the preparation of NH_3-MMT and NH_2-MMT.

FTIR Analysis. The FTIR spectra of MMT, NH_2-MMT, and P-NH_2-MMT are shown in Figure 2. According to previous studies,[12,13] silane coupling agent can be covalently bonded to the surface of MMT platelets. The characteristic peak between 3200 and 3300 cm^{-1} was attributed to the stretching of the primary amino group (—NH_2).[18] Moreover, the appearance of a new band at 2940 cm^{-1} due to the C—H stretching vibration of APTS indicates the attachment of APTS to MMT. For P-NH_2-MMT, two strong peaks at 2929 and 2860 cm^{-1}, which are attributed to the C—H stretching vibration in TTP. Moreover, the relative intensities of the bands at 3431 and 1639 cm^{-1} decrease because of the decrease of the amount of water in the interlayer after the intercalation of TTP, which makes MMT less hydrophilic.

TGA. TGA was performed to determine the organic content and the degradation behavior of the modified MMT. As shown in Figure 3(a), ~6.8 wt % of mass loss occurs for pristine MMT at temperature below 200°C, which can be attributed to the release of physically adsorbed water. Similarly, about 5.9 wt % of mass loss for NH_2-MMT was observed at temperature below 200°C. On the other hand, P-NH_2-MMT, the double-modified MMT, exhibits much better thermal stability below 300°C than MMT and NH_2-MMT. In Figure 3(b), the differential TG (DTG) curves of both MMT and NH_2-MMT show a peak below 200°C, whereas P-NH_2-MMT shows no peak below 200°C, indicating that P-NH_2-MMT intercalated by TTP is much less hydrophilic, which is obviously in favor of the structural stability of P-NH_2-MMT during melt blending. At temperatures above 300°C, the thermal degradation of P-NH_2-MMT is accelerated. The organosilyl groups grafted to the silicates are highly stable and start decomposing only at above 400°C.[22,23] As for NH_2-MMT, there is a broad peak at 430°C, which should be attributed to the release of degradation products of the grafted APTS. The mass loss temperature above 600°C has been previously assigned to the loss of structural hydroxyl water from MMT.[24] P-NH_2-MMT shows major peaks at 401, 468, and 501°C, which should be attributed to the release of the degradation products of TTP ions.

Structure and Properties of PP/MMT Nanocomposites

XRD Analysis. As aforementioned, P-NH_2-MMT shows a strong peak at 3.96°, corresponding to a basal space of 2.23 nm (Figure 1). When 3 wt % of P-NH_2-MMT was incorporated

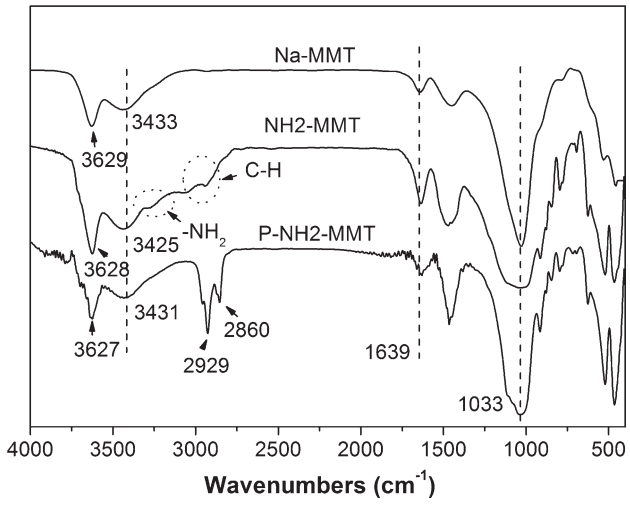

Figure 2. FTIR spectra of MMT, NH_2-MMT, and P-NH_2-MMT.

Applied Polymer SCIENCE

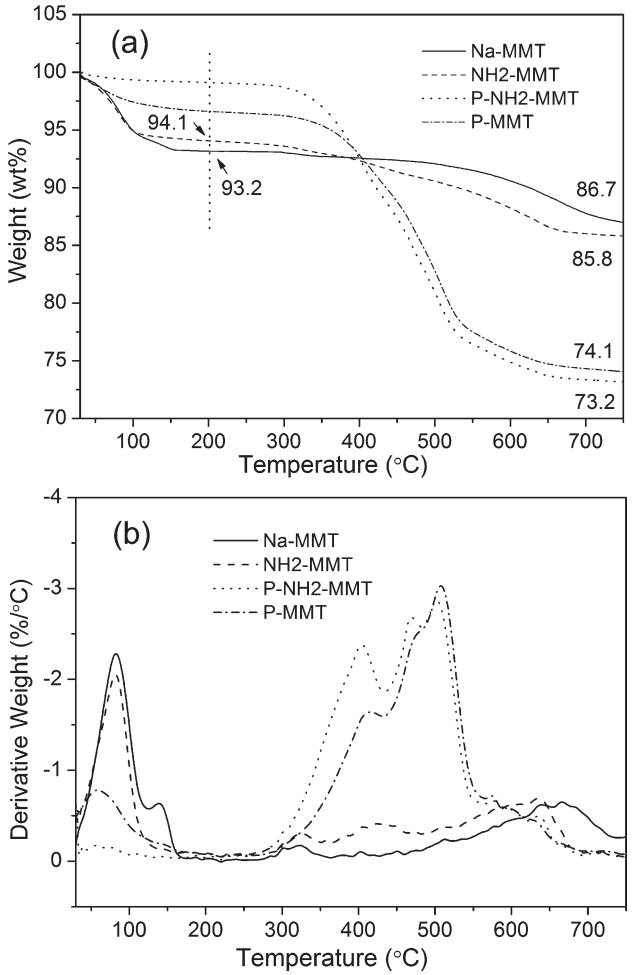

Figure 3. TG (a) and DTG (b) curves of pristine MMT and the modified MMTs.

into PP-0, the diffraction peak shifts to 3.29°, corresponding to a 2.68 nm basal space, as shown in Figure 4. This suggests that PP macromolecular chains may enter the gallery space and enlarge the gallery space. The influence of PP-*g*-MA on the structure of P-NH_2-MMT/PP nanocomposites is complicated. In Figure 4, PP-2 and PP-4 show the characteristic diffraction peaks at $2\theta = 3.22°$ and 3.69°, respectively, corresponding to the basal space (d_{001}) of 2.74 and 2.40 nm, respectively. The basal space of PP-2 is similar with that of PP-0, whereas for PP-4, it is slightly smaller than that of PP-0. However, it should be noted that the intensity of the diffraction peak is greatly decreased with the increase of PP-*g*-MA content. When the content of PP-*g*-MA is further increased to 6 wt %, no diffraction peak can be observed. The reduction of the diffraction intensity should be attributed to the exfoliation of MMT in the matrix.[25,26]

To understand the effect of APTS on the structure of the nanocomposites, the XRD patterns of P-MMT and PP-P-6, the control samples, were recorded, as shown in Figure 5. P-MMT has a basal space (d_{001}) of 2.20 nm, which is similar to that of P-NH_2-MMT. Therefore, it seems that the influence of APTS on the basal space of modified MMT is limited. However, PP-P-6

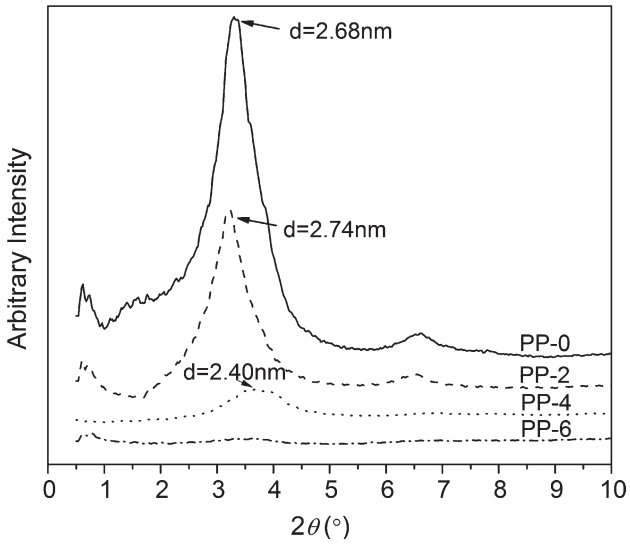

Figure 4. XRD patterns of PP/MMT nanocomposites.

nanocomposite shows a strong peak at 5.05°, corresponding to a 1.75 nm basal space, which is much smaller than that of P-MMT. A possible explanation to this phenomenon is as follows: P-MMT is only decorated by TTP cations, therefore, different from P-NH_2-MMT, which contains amine groups and is reactive with PP-*g*-MA and brings about the exfoliation of P-NH_2-MMT in PP, and the platelets of P-MMT are squeezed during the melt blending process. By comparing PP-P-6 and PP-6 nanocomposites, one can speculate that the modification of MMT by APTS greatly contributes to the improved dispersion of MMT in PP matrix in the existence of PP-*g*-MA.

Morphology of the Nanocomposites. TEM is further used to illuminate the morphology of the nanocomposites. TEM images of PP/P-NH_2-MMT nanocomposites at different concentrations of PP-*g*-MA are shown in Figure 6. In the absence of PP-*g*-MA, MMT is unexfoliated and agglomerated. When PP-*g*-MA is introduced into the PP/MMT nanocomposites, the particle size of MMT becomes much smaller [Figure 6(c, d)]. For PP-6 containing 6 wt % of PP-*g*-MA, the double-modified MMT is less

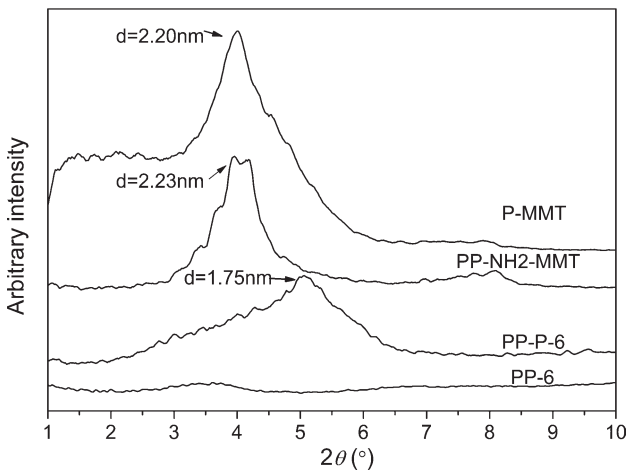

Figure 5. XRD patterns of P-MMT, P-NH_2-MMT, PP-P-6, and PP-6.

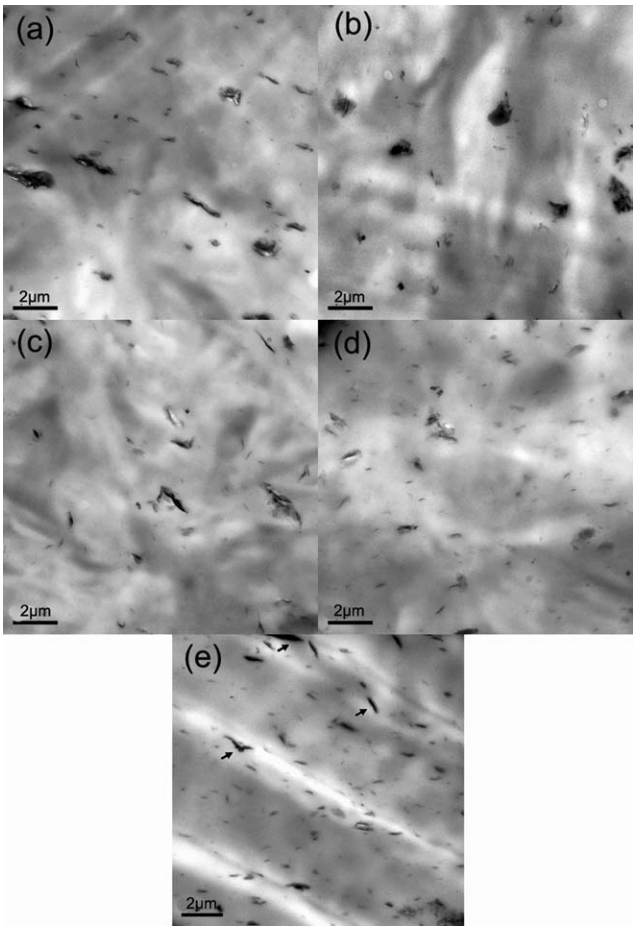

Figure 6. TEM images of PP/P-NH_2-MMT nanocomposites: (a) PP-0; (b) PP-2; (c) PP-4; (d) PP-6; and (e) PP-P-6.

agglomerated and disperses uniformly in the matrix [Figure 6(d)]. For P-MMT that does not contain amine groups, its dispersion is less uniform and there are more agglomerates in the TEM image, as denoted by the arrows in Figure 6(e). This is consistent with the results of XRD. Figure 7 further shows the TEM image of PP-6 nanocomposites at a high magnification. As denoted by the arrows, both exfoliated MMT sheets and intercalated MMT particles are observed, which disperse homogenously in the matrix. Because the primary amino groups of the double-modified MMT can react with the anhydride groups of PP-*g*-MA during melt blending,[27,28] the PP chains should be able to be grafted to the surfaces of MMT sheets. According to Gianni et al.,[29] the interaction between silane coupling agents and epoxy resins is able to bring about the intercalation epoxy into the silicate galleries, which is in good agreement with our observation. This demonstrates that the double-modified MMT can disperse more uniformly in PP in the existence of PP-*g*-MA.

Thermal Properties. The TG and the corresponding DTG curves for PP and PP/MMT nanocomposites in nitrogen are shown in Figure 8. The initial degradation temperature corresponding to a weight loss of 5 wt % ($T_{0.05}$) and maximum mass loss temperature (T_{max}) for the samples are summarized

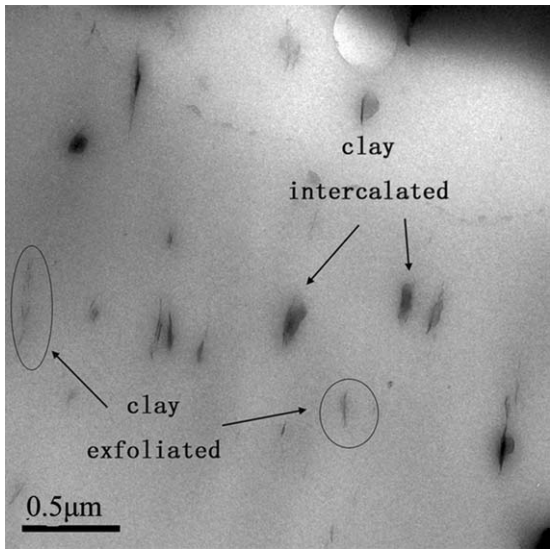

Figure 7. TEM image of PP-6 nanocomposite at a high magnification.

in Figure 8(a). The thermal stability of PP is improved by the incorporation of both the double-modified MMT and TTPC-modified MMT. The $T_{0.05}$ of the nanocomposites ranges from

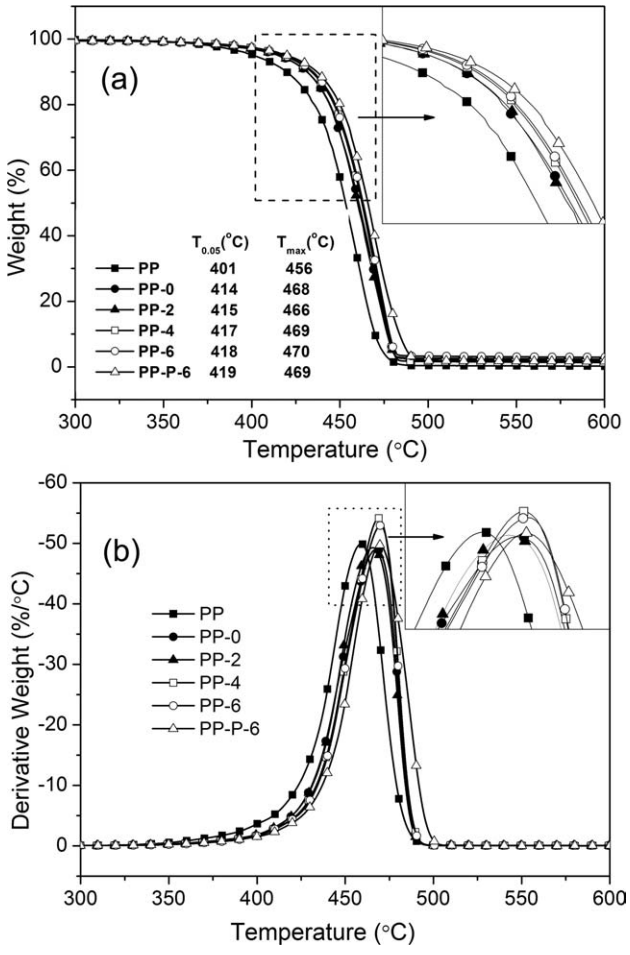

Figure 8. TG (a) and DTG (b) curves of PP and PP/MMT nanocomposites under nitrogen (heating rate 20°C min^{-1}).

Applied Polymer SCIENCE

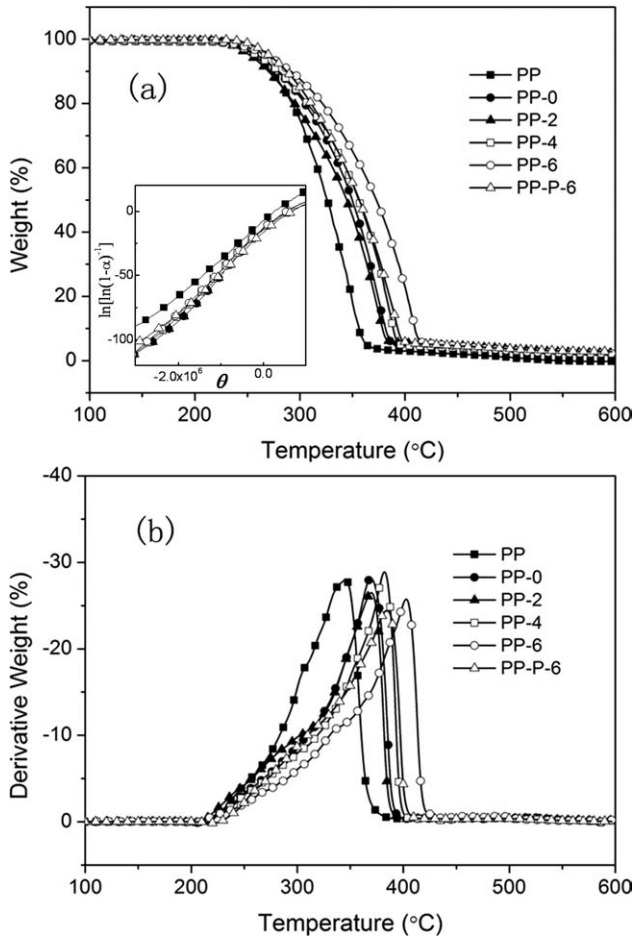

Figure 9. TG (a) and DTG (b) curves of PP and PP/MMT nanocomposites under air (heating rate 20°C min^{-1}). The inset of (a) shows the plots of $\ln[\ln(1-\alpha)^{-1}]$ versus θ for the calculation of E_a.

414 to 419°C, and T_{max} is around 468°C. In contrast, pure PP has a $T_{0.05}$ of about 401°C and a T_{max} of 456°C. This result indicates that MMT was able to enhance the thermal stability of PP/MMT nanocomposites in nitrogen.

Furthermore, because polymers are usually used in air condition, from the view of practical application, it is important to evaluate the thermal properties of the samples in air. The TG and DTG curves for PP and its nanocomposites in air are shown in Figure 9, and the detailed data are summarized in Table II. The initial decomposition temperature ($T_{0.05}$) of PP is about 255°C, and the maximum mass loss peak (T_{max}) is at about 344°C. Obviously, the presence of P-NH_2-MMT, the double-modified MMT, retards the oxidative degradation of PP. Previous studies have shown that MMT was believed to be able to improve the flame retardancy and thermal properties of polymers by forming a continuous and compact network on the surface of the polymers.[30,31] The result also shows that PP-*g*-MA has noted influence on the thermal stability of the PP/MMT nanocomposites. In the absence of PP-*g*-MA, the $T_{0.05}$ and T_{max} values for PP-0 were around 259 and 369°C, respectively, which are 4 and 25°C higher than those of PP. With the increased content of PP-*g*-MA, the $T_{0.05}$ and T_{max} values of the nanocomposites are noticeably increased. For PP-6 containing 6 wt % of PP-*g*-MA, the TG curve [Figure 10(a)] shifts to higher temperatures, and the $T_{0.05}$ and T_{max} values are around 267 and 403°C, respectively, which are about 12 and 55°C higher than those of PP and are 8 and 30°C higher than those of PP-0. Because PP-*g*-MA by itself has little effect on the decomposition behavior of pure PP, the above results suggest that PP-*g*-MA improves the dispersion of P-NH_2-MMT in PP and thus facilitates the formation of barrier layer when the samples are exposed to high temperatures.

As to PP-P-6 filled with P-MMT, the TTPC-modified MMT, the $T_{0.05}$ and T_{max} are about 270 and 385°C, respectively, that is, about 15 and 41°C higher than those of PP. $T_{0.05}$ is about 3°C higher than that of PP-6, whereas $T_{0.1}$, $T_{0.5}$, and T_{max} are obviously lower than those of PP-6, indicating that the P-MMT is not as effective as P-NH_2-MMT with the increase in the thermal stability of PP in air. As aforementioned, the dispersion of P-NH_2-MMT is more uniform than P-MMT in PP and more P-NH_2-MMT are exfoliated in PP matrix. These factors are responsible for the improved thermal stability.

As for the activation energy (E_a), it was observed that the E_a of the PP/MMT nanocomposites is larger than that of pure PP, which suggests that the presence of MMT increases the threshold of thermal oxidative degradation of PP. This result is in good agreement with previous study,[32] which shows that the nanodispersed silicate layers decrease the decomposition rate and increase the temperature of degradation by acting as an excellent thermal insulation and mass transport barrier.

PP and the PP/MMT nanocomposites were heated at 380°C for 5 min in a muffle furnace. As shown in Figure 10, after the heat

Table II. TG and DTG Results Under Air Atmosphere for Pure PP and Its Nanocomposites

Sample code	$T_{0.05}$[a] (°C)	$T_{0.10}$[a] (°C)	$T_{0.50}$[a] (°C)	T_{max}[a] (°C)	$\Delta T_{0.05}$ (°C)	$\Delta T_{0.10}$ (°C)	$\Delta T_{0.50}$ (°C)	ΔT_{max} (°C)	E_a (kJ mol^{-1})
PP	255	271	324	344	NA	NA	NA	NA	23.9
PP-0	259	279	350	369	4	8	26	25	25.0
PP-2	252	269	344	370	−3	−2	20	26	25.4
PP-4	259	279	356	382	4	8	32	38	25.4
PP-6	267	291	374	403	12	20	50	59	26.2
PP-P-6	270	287	356	385	15	16	32	41	25.7

[a]$T_{0.05}$, $T_{0.10}$, and $T_{0.50}$: temperatures at which 5, 10, and 50 wt % weight loss occurs; T_{max}, the maximum weight loss rate temperature.

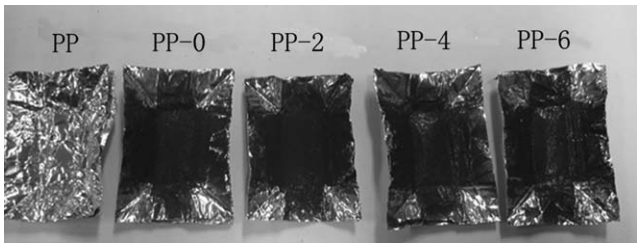

Figure 10. Digital photographs of PP and PP/P-NH_2-MMT nanocomposites, which were heated at 380°C for 5 min.

treatment, pure PP almost decomposed completely almost leaving no residue, whereas the PP/P-NH_2-MMT nanocomposites left some black residue on the aluminum foils, and the residues are relatively uniform and compact.

To further investigate the relationship between the microstructure of MMT layers and the thermal performance, the morphologies of the residues after the heat treatment at 380°C were characterized by SEM as shown in Figure 11. In the combustion of polymers, char layer can function as the protecting "coating" of the materials and delay the volatilization of combustible gases and retard the penetration of oxygen and feedback of heat flux. In case the polymer does not form a char layer by itself, the MMT "char" would play the major role in preventing the heat transfer and mass loss.[33] Figure 11 shows that the residue of PP-0, PP-2, and PP-4 contains some holes and cracks on the surface, whereas the residues of PP-6 are more compact and less cracks can be observed on the surface. This indicates that a more efficient protective residue layer forms for PP-6 because of the higher loading of PP-*g*-MA and the improved dispersion of P-NH_2-MMT, which explains the improved heat resistance of PP-6 in air.

Figure 12 shows the FTIR spectra of the residue of PP/MMT nanocomposites. The absorption at 1050 cm^{-1} is Si—O stretching vibration of P-NH_2-MMT. The peaks around 2900 cm^{-1} are C—H stretching vibration. There are no peaks around 2900 cm^{-1} for PP-0-t and PP-2-t, in contrast to PP-4-t and PP-6-t. It indicates that the residue of PP-4 and PP-6 contains hydrocarbon alkyl substituents, which may be attributed to the increased amount of polymer grafted on the surface of MMT platelets or enter the interlayer of MMT at a relatively high PP-*g*-MA content. The polymer inside the interlayer of MMT can be well protected by the MMT platelets from heat and oxygen during the heat treatment.

Mechanical Properties. To shed light on the effect of double-modified MMT on the mechanical properties of PP/MMT nanocomposites, the stress–strain curves of PP and PP/MMT nanocomposites were measured as shown in Figure 13. Neat PP exhibits a distinct yield point and very large elongation at break. On the contrary, the PP/MMT nanocomposites exhibit greatly

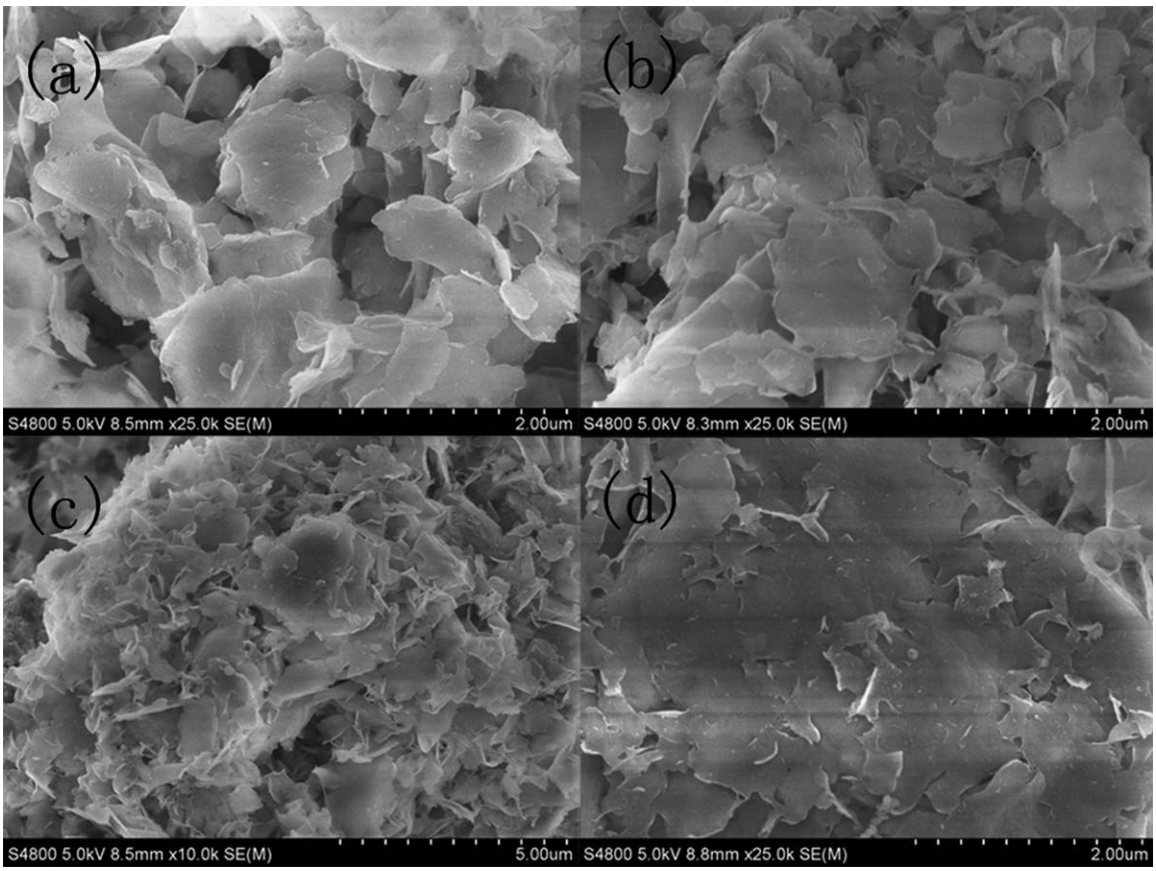

Figure 11. SEM images of the residue of PP/MMT nanocomposites, which were heated at 380°C for 5 min in a muffle furnace: (a) PP-0; (b) PP-2; (c) PP-4; and (d) PP-6.

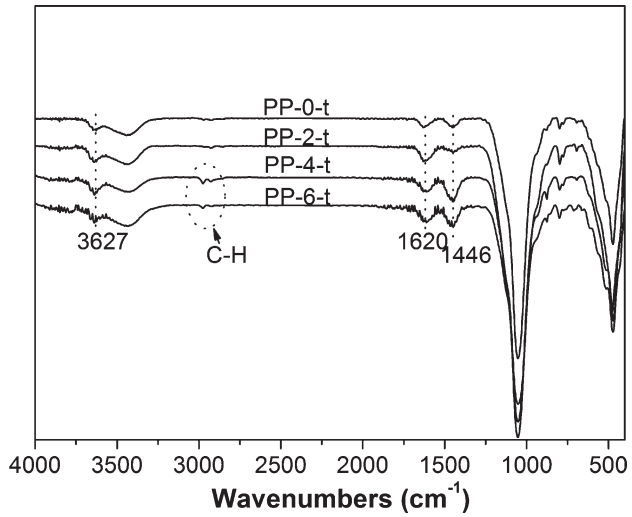

Figure 12. FTIR spectra of the residues of PP-0, PP-2, PP-4, and PP-6 nanocomposites (designated as PP-0-t, PP-2-t, PP-4-t, and PP-6-t, respectively).

decreased elongation at break. However, the tensile strength and the Young's modulus are significantly increased by the introduction of double-modified MMT and PP-*g*-MA. The improvement of Young's modulus can be associated with the constraining effects of the MMT platelets on the motion of polymer chains, the high aspect ratio, and the degree of dispersion of MMT. It should be noted that with the increase of the content of PP-*g*-MA, the mechanical properties are increased, and PP-6 containing both the double-modified MMT and PP-*g*-MA exhibit the best mechanical properties. For example, the tensile strength and Young's modulus of PP-6 shows an increase of 16.5% and 28%, respectively, when compared with those of PP-0 that contain the double-modified MMT but does not contain PP-*g*-MA. The tensile strength and the Young's modulus of PP-6 are 18% and 23% higher than those of PP-P-6, respectively. The latter contains PP-*g*-MA and TTPC-modified MMT instead of the double-modified MMT. The improvement of the mechanical properties of PP-6 is attributed to the improved interfacial

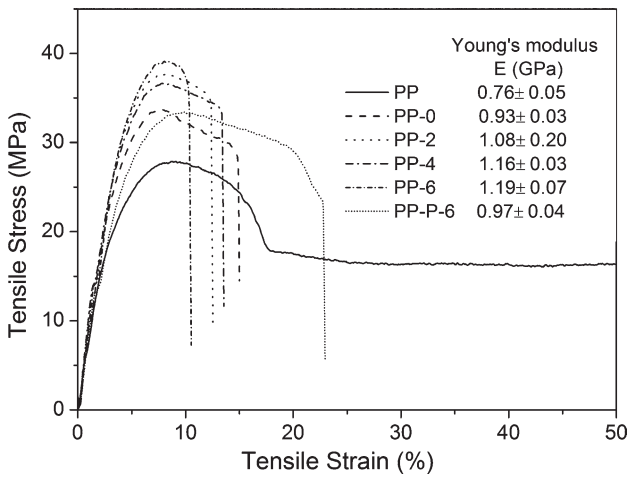

Figure 13. Stress–strain curves of neat PP and PP/MMT nanocomposites.

interaction between the double-modified MMT and PP matrix, as well as the better intercalation and exfoliation behavior of P-NH_2-MMT in PP matrix in the existence of PP-*g*-MA.

CONCLUSION

In this work, the influence of PP-*g*-MA on the dispersion of double-modified MMT in PP and the thermal and mechanical properties of the PP/MMT nanocomposites were investigated. It was found that PP-*g*-MA can greatly improve the dispersion of the double-modified MMT in PP. In the existence of PP-*g*-MA, the platelets of the double-modified MMT are partially intercalated and partially exfoliated in the nanocomposites. Furthermore, the PP/MMT nanocomposites with PP-*g*-MA exhibit both improved thermal stability and mechanical properties when compared with neat PP and PP/MMT nanocomposite without PP-*g*-MA because of the improved dispersion of MMT.

ACKNOWLEDGMENTS

This work was supported by the Program for Zhejiang Provincial Innovative Research Team, China (no.: 2009R50004).

REFERENCES

1. Usuki, A.; Kawasumi, M.; Kojima, Y.; Fukushima, Y.; Okada, A.; Kurauchi, T.; Kamigaito, O. *J. Mater. Res.* **1993,** *8*, 1179.
2. Lee, S. R.; Park, H. M.; Lim, H.; Kang, T.; Li, X.; Cho, W. J.; Ha, C. S. *Polymer* **2002,** *43*, 2495.
3. Okamoto, M.; Morita, S.; Taguchi, H.; Kim, Y. H.; Kotato, T.; Tateyama, H. *Polymer* **2000,** *41*, 3887.
4. Lan, T.; Pinnavaia, T. *Chem. Mater.* **1994,** *6*, 2216.
5. Peng, M.; Li, H. B.; Wu, L. J.; Chen, Y.; Zheng, Q.; Gu, W. F. *Polymer* **2005,** *46*, 7612.
6. Peng, M.; Li, D. S.; Chen, Y.; Zheng, Q. *J. Appl. Polym. Sci.* **2007,** *104*, 1205.
7. Zhao, Z. F.; Tang, T.; Qin, Y. X.; Huang, B. T. *Langmuir* **2003,** *19*, 7157.
8. Stockmeyer, M. R. *Appl. Clay Sci.* **1991,** *6*, 39.
9. Velde, B. Introduction to Clay Minerals; Chapman and Hall: London, **1992.**
10. Xiao, J. F.; Hu, Y.; Wang, Z. H.; Tang, Y.; Chen, Z. Y.; Fan, W. C. *Eur. Polym. J.* **2005,** *41*, 1030.
11. Stoeffler, K.; Lafleur, P. G.; Denault, J. *Polym. Degrad. Stab.* **2008,** *93*, 1332.
12. Wang, K.; Wang, L.; Wu, J.; Chen, L.; He, C. *Langmuir* **2005,** *21*, 3613.
13. Chow, W. S.; Neoh, S. S. *J. Appl. Polym. Sci.* **2009,** *114*, 3967.
14. Manias, E.; Touny, A.; Wu, L.; Strawhecker, K.; Lu, B.; Chung, T. C. *Chem. Mater.* **2001,** *13*, 3516.
15. Hasegawa, N.; Kawasumi, M.; Kato, M.; Usuki, A.; Okada, A. *J. Appl. Polym. Sci.* **1998,** *67*, 87.
16. Kato, M.; Usuki, A.; Okada, A. *J. Appl. Polym. Sci.* **1997,** *66*, 1781.
17. Hasegawa, N.; Okamato, H.; Kato, M.; Usuki, A. *J. Appl. Polym. Sci.* **2000,** *78*, 1918.

18. Liaw, W. C.; Huang, P. C.; Chen, C. S.; Lo, C. L.; Chang, J. L. *J. Appl. Polym. Sci.* **2008,** *109*, 1871.
19. Wu, C. S.; Liu, Y. L.; Chiu, Y. C.; Chiu, Y. S. *Polym. Degrad. Stab.* **2002,** *78*, 41.
20. Park, S. J.; Kim, H. C.; Lee, H. I.; Suh, D. H. *Macromolecules* **2001,** *34*, 7573.
21. Horowitz, H. H.; Metzger, G. *Anal. Chem.* **1963,** *35*, 1464.
22. Ruizhitzky, E.; Rojo, J. M. *Nature* **1980,** *287*, 28.
23. Ogawa, M.; Miyoshi, M.; Kuroda, K. *Chem. Mater.* **1998,** *10*, 3787.
24. Olphen, H. V. An Introduction to Clay Colloid Chemistry; Wiley: New York, **1977;** Vol. *2*.
25. Lee, K. M.; Han, C. D. *Polymer* **2003,** *44*, 4573.
26. Du, B. X.; Guo, Z. H.; Fang, Z. P. *Polym. Degrad. Stab.* **2009,** *94*, 1979.
27. Colbeaux, A.; Fenouillot, F.; Gerard, J. F.; Taha, M.; Wautier, H. *Polym. Int.* **2005,** *54*, 692.
28. Cui, L. L.; Paul, D. R. *Polymer* **2007,** *48*, 1632.
29. Di Gianni, A.; Amerio, E.; Monticelli, O.; Bongiovanni, R. *Appl. Clay Sci.* **2008,** *42*, 116.
30. Zhu, J.; Wilkie, C. A. *Polym. Int.* **2000,** *49*, 1158.
31. Ma, H. Y.; Tong, L. F.; Xu, Z. B.; Fang, Z. P. *Polym. Degrad. Stab.* **2007,** *92*, 1439.
32. Qin, H. L.; Zhang, S. M.; Zhao, C. G.; Hu, G. J.; Yang, M. S. *Polymer* **2005,** *46*, 8386.
33. Pack, S.; Kashiwagi, T.; Cao, C. H.; Korach, C. S.; Lewin, M.; Rafailovich, M. H. *Macromolecules* **2010,** *43*, 5338.